Quantitative photoacoustic imaging: fitting a model of light transport to the initial pressure distribution

B. T. Cox[a], S. R. Arridge[b], K. P. Köstli[a] and P. C. Beard[a]

[a] Department of Medical Physics and Bioengineering, University College London, Gower Street, London WC1E 6BT, UK

[b] Department of Computer Science, University College London, Gower Street, London WC1E 6BT, UK

ABSTRACT

Photoacoustic imaging, which generates a map of the initial acoustic pressure distribution generated by a short laser pulse, has been demonstrated by several authors. *Quantitative* photoacoustic imaging takes this one stage further to produce a map of the distribution of an optical property of the tissue, in this case absorption, which can then be related to a physiological parameter. In this technique, the initial pressure distribution is assumed to be proportional to the absorbed laser energy density. A model of light transport in scattering media is then used to estimate the distribution of optical properties that would result in such a pattern of absorbed energy. The light model used a finite element implementation of the diffusion equation (with the δ-E(3) approximation included to improve the accuracy at short distances inside the scattering medium). An algorithm which applies this model iteratively and converges on a quantitative estimate of the optical absorption distribution is described. 2D examples using simulated data (initial pressure maps) with and without noise are shown to converge quickly and accurately.

Keywords: photoacoustic, quantitative imaging, optical absorption coefficient

1. INTRODUCTION

In biomedical photoacoustic imaging, the spatially-varying pressure increase following the absorption of a laser pulse is reconstructed from time-resolved measurements of the subsequent acoustic radiation recorded over the tissue surface. For a short pulse, this image of the initial pressure distribution is proportional to the absorbed optical energy density. As this is the product of both the local absorption coefficient and the fluence distribution, it provides only an indirect representation of the tissue optical properties. However, it is the optical properties that reflect the tissue structure and physiology. In the algorithm described here, we address this by recovering the distribution of *optical absorption* from the image of the absorbed optical energy using an iteratively applied forward model of light transport. As this produces a map of the optical absorption coefficient in absolute units it will be referred to as *quantitative* photoacoustic imaging.

There are several distinct advantages of this approach. First, the absorption coefficient distribution, unlike the absorbed energy map, is directly related to the spatial distribution of absorbing tissue chromophores and does not depend on the fluence. This provides for a more representative image contrast distribution and a more straightforward visual interpretation e.g. it removes the depth-dependent fall-off due to optical attenuation.

Second, quantitative absorption images are directly relevant to spectroscopic imaging applications, where the objective is to recover the local absorption spectra of specific chromophores such as oxy and deoxy hemoglobin (for the measurement of blood oxygenation)[1,2] or contrast agents such as those used in photoacoustic molecular imaging.[3] Obtaining such spectroscopic information directly from multiwavelength images of the absorbed energy distribution with sufficient accuracy can be problematic due to the influence of the wavelength dependence of the internal light distribution. This results in the spectroscopic characteristics of different regions becoming coupled.[2] For example, the characteristic spectral signature of a superficial blood vessel will be encoded onto,

Send correspondence to B. T. Cox. bencox@medphys.ucl.ac.uk

Proc. SPIE **5697**, 49-55
SPIE BIOS 2005, 23-25 January 2005, San Jose, USA

and thereby distort, that of a vessel lying directly beneath it. Reconstructing images in terms of the absolute or even relative absorption coefficient avoids this.

Finally, since the image is quantitatively reconstructed in units of optical absorption it offers the prospect of making comparisons over time of absolute changes in physiological parameters.

Paltauf and Schmidt-Kloiber[4] have inverted photoacoustic signals for optical absorption. They describe two methods for estimating the depth-dependent absorption in a layered (1D), non-scattering medium, from PA time series measured in the acoustic near and far field. This paper describes a simple iterative method for estimating a 2D absorption distribution from the absorbed energy distribution in a scattering medium.

2. PHOTOACOUSTIC IMAGING

If a region of a fluid is heated through the absorption of a laser pulse, a sound wave is generated. In a stationary fluid with isotropic acoustic properties, under conditions whereby the sound generation mechanism is thermoelastic and we can neglect the effects of viscosity and thermal conductivity, the wave equation for the acoustic pressure is

$$\nabla^2 p - \frac{1}{c^2}\frac{\partial^2 p}{\partial t^2} = \frac{-\beta}{C_p}\frac{\partial \mathcal{H}}{\partial t} \tag{1}$$

where c is the sound speed, β is the volume thermal expansivity, C_p is the constant pressure specific heat capacity and $\mathcal{H}$ is the heat energy per unit volume and per unit time deposited in the fluid. p and $\mathcal{H}$ will depend, in general, on the position $\mathbf{x} = (x, y, z)$ and time t. When the laser pulse is effectively instantaneous (the stress confinement condition is met) the heating function can be modelled as

$$\mathcal{H}(\mathbf{x}, t) = H(\mathbf{x})\delta(t) \tag{2}$$

where $H(\mathbf{x})$ is the heat deposited in the fluid per unit volume. The heating is due to the absorbed laser energy. If the light fluence at a point in the fluid is $F(\mathbf{x}, t)$ and the absorption coefficient distribution $\mu_a(\mathbf{x})$ then the spatial part of the heating function can be written as

$$H(\mathbf{x}) = \mu_a(\mathbf{x})F(\mathbf{x}, \mu_a) \tag{3}$$

The heating function or deposited energy density, $H(\mathbf{x})$, is also called the distribution of absorbed optical energy or just the absorbed energy map. The fluence F will in general depend on the absorption coefficient distribution $\mu_a(\mathbf{x})$ and the scattering coefficient distribution $\mu_s'(\mathbf{x})$ and hence the absorbed energy H is *non-linearly* related to μ_a. In the case of δ-function heating, Eq. (2), the optical energy will be absorbed before the fluid density has time to change. In this case, the acoustic pressure immediately following the pulse, or initial pressure distribution, $p_0(\mathbf{x})$, is proportional to the absorbed energy map

$$p_0(\mathbf{x}) = \left(\frac{\beta c^2}{C_p}\right) H(\mathbf{x}) = \Gamma H(\mathbf{x}) \tag{4}$$

Γ is the Grüneisen coefficient, a dimensionless constant that represents the efficiency of the conversion of heat to pressure. ($\Gamma \approx 0.11$ for water at standard temperature and pressure.) This initial pressure distribution then propagates away as acoustic waves according to Eq. (1). 'Conventional' biomedical photoacoustic imaging measures these acoustic waves over the tissue surface as a function of time, and backpropagates them to obtain an image proportional to the initial pressure distribution, or absorbed energy map.[5–7] The map of the distribution of absorbed energy density that is recovered from the acoustic measurements will be called the *measured* absorbed energy map and denoted $\hat{H}$. In this paper it is used as the starting point for the quantitative estimation of the absorption distribution and is simulated using a numerical model of light transport.

3. QUANTITATIVE ESTIMATION OF ABSORPTION DISTRIBUTIONS

In general, the measured absorbed energy map, Eq. (3) will not be proportional to the absorption coefficient distribution. If the fluence distribution is known then the absorption coefficient distribution can be calculated from the absorbed energy map, but this is not usually the case. If the fluence is constant over the image plane - this may almost be the case for a plane perpendicular to the incident light pulse, for instance[8] - then the absorbed energy map is *proportional* to the absorption coefficient distribution, but even in this case the fluence must be known for a quantitative estimate of the absorption. In this section we describe a method of fitting a model of light transport to the measured absorbed energy map in order to recover the absorption coefficient distribution in absolute units.

The absorbed energy at a point $\mathbf{x}$, $H(\mathbf{x})$, is not only a non-linear function of the absorption at that point $\mu_a(\mathbf{x})$, as mentioned above, but also - via the fluence - depends on the absorption at other, nearby, points. Recovering μ_a from a measurement of H is therefore a non-trivial problem. However, if $\hat{H}$ is measured in absolute units, the input light distribution in known, and a realistic scattering coefficient distribution μ_s' can be assumed then the absorption distribution may be recovered using the following scheme based on fixed-point iteration: (1) Choose an estimate for the initial absorption distribution, eg. $\mu_a^{(0)} = 0$ for iteration number $k = 0$. (2) Calculate the fluence and absorbed energy distributions, $\Phi^{(k)}$ and $H^{(k)}$, that would be produced by $\mu_a^{(k)}$, using a model of the propagation of light in a scattering medium. (3) Calculate the next estimate of the absorption coefficient using $\mu_a^{(k+1)} = \hat{H}/\Phi^{(k)}$. (4) Iterate steps (2) and (3) until the difference between the measured and calculated absorbed energy maps, $\Delta H^{(k)} = \hat{H} - H^{(k)}$, is sufficiently small. This is shown in the flowchart in Figure 1.

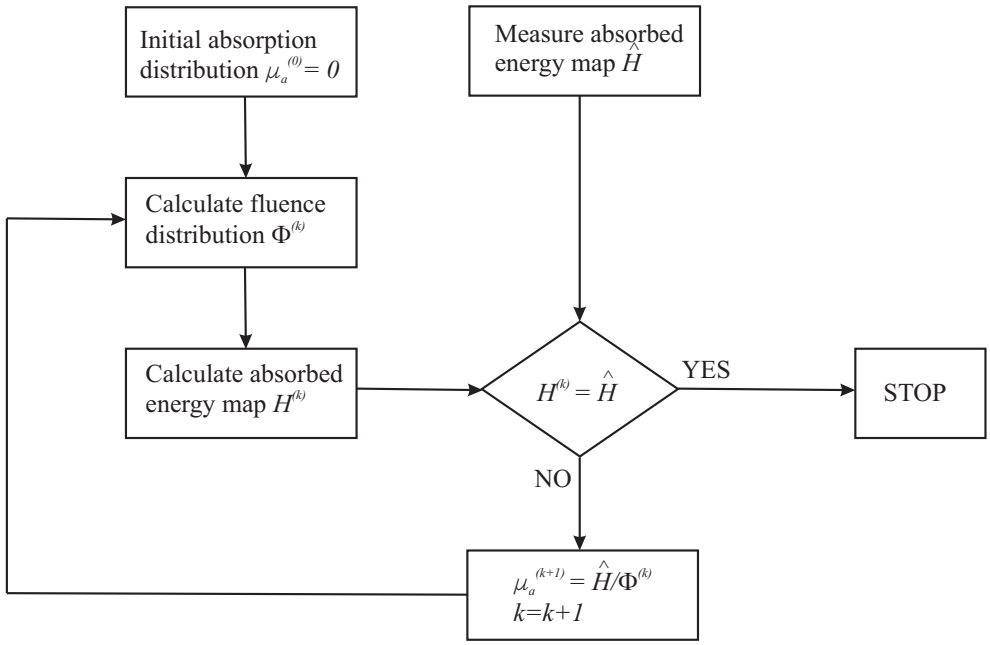

Figure 1. Flowchart showing the quantitative photoacoustic imaging algorithm

3.1. Forward Model

In order to calculate the fluence estimate in step (2), a fast and accurate model of the propagation of light in turbid media is required. The diffusion approximation to the transport equation, with the δ-E(3) approximation to improve the accuracy at distances close to the illuminated surface of the scattering medium,[9] was implemented using the finite-element (FE) method.[10] (By including the δ-E(3) approximation, which shifts a

proportion of the scattered light into the forward direction, the fluence distributions calculated from this model are comparable in accuracy to results using Monte-Carlo simulation even for short penetration depths.) In the examples below, this FE model was used both to simulate the 'measured' absorbed energy distribution and to estimate the fluence in step (2).

Two examples are considered below: a noise-free example to test the algorithm converges to an unbiased estimate of the absorption, and a more realistic noisy case. In the noise-free example, a 2D 70×70 grid was used for both these steps. However, for the more realistic noisy case, in order to avoid the 'inverse crime' of using the same grid for generating and recovering the data (and thereby providing the inversion with some prior knowledge), the simulated data was calculated on a 151×151 grid first and then interpolated to a non-coincident 70×70 grid which was used for the iterative estimations. In both examples, the illuminating beam has a top-hat profile of radius 4 mm and is incident from the left of the image. The scattering coefficient μ_s was set throughout to be 5 mm^{-1} and the anisotropy factor to 0.8. Three absorbing features were included in a background absorption of 0.01 mm^{-1}, a small circle 0.4 mm^{-1}, a large circle 0.1 mm^{-1} and a rectangle 0.15 mm^{-1}. These absorption coefficients are typical of the absorption of near-infrared light in human blood and soft tissue.

3.2. 2D noise-free example

When the measured $\hat{H}$ is noise-free, as it can be only in a simulation, the algorithm should recover the absorption coefficient distribution exactly. In other words, the inversion algorithm should converge to the correct solution and introduce no bias into the estimate of the absorption. This was shown to be the case in the example in Figure 2. The absorption coefficient distribution (top left) was used to calculate the absorbed energy map (top right) which was used as input to the iteration scheme to estimate the absorption (middle left: map, middle right: profiles). The fluence (bottom left) is also estimated. A measure of the error after each iteration, $\log_{10} \|\Delta H\|$ (bottom left) shows that the error rapidly decreases and is negligible after 20 iterations. Each iteration took < 1 second on a PC with a 2GHz processor.

3.3. 2D example with noise: regularisation

A more realistic example may be simulated by including noise in the 'measured' absorbed energy map. Figure 3 shows the same example as in Figure 1 but with noise. Two types of noise are included: noise due to the interpolation from a large to a smaller grid as described above, and additive Gaussian noise. The signal-to-noise ratio (SNR) in the noisy absorbed energy map will vary from point to point depending on the absorption and the fluence distributions. In this example it varies in the range 50dB to -20 dB. In regions where the fluence estimate $\Phi^{(k)}$ is low, the absorption coefficient estimate $\mu_a^{(k+1)} = \hat{H}/\Phi^{(k)}$ becomes very sensitive to errors in the measured energy map $\hat{H}$. As $\hat{H}$ now contains noise it is necessary to include a regularisation term to limit this instability. To this effect, we calculate the absorption estimate in step (3) using a regularisation parameter σ:

$$\mu_a^{(k)} = \frac{\hat{H}}{\Phi^{(k)} + \sigma} \tag{5}$$

σ could, in general, be spatially-varying, but here was chosen as the value of the absorbed energy for an SNR of 0 dB.

The results in Figure 3 show that the absorption coefficient distribution can be estimated in the presence of noise, although the estimate becomes inaccurate where the SNR is low. The circles of absorption in the recovered distribution have rougher boundaries than the true absorption distribution. This is due to the interpolation to a coarser grid and does not represent a trade-off between shape accuracy and absorption coefficient accuracy. The bottom-right graph in Figure 3 shows the log of the mean-squared difference between the 'measured' and estimated absorbed energy distributions, effectively a combined measure of the average error in the fluence and absorption estimates. When this converges (as in this case) it converges towards a minimum which, for a given absorption distribution, depends on the SNR and the value of the regularisation parameter.

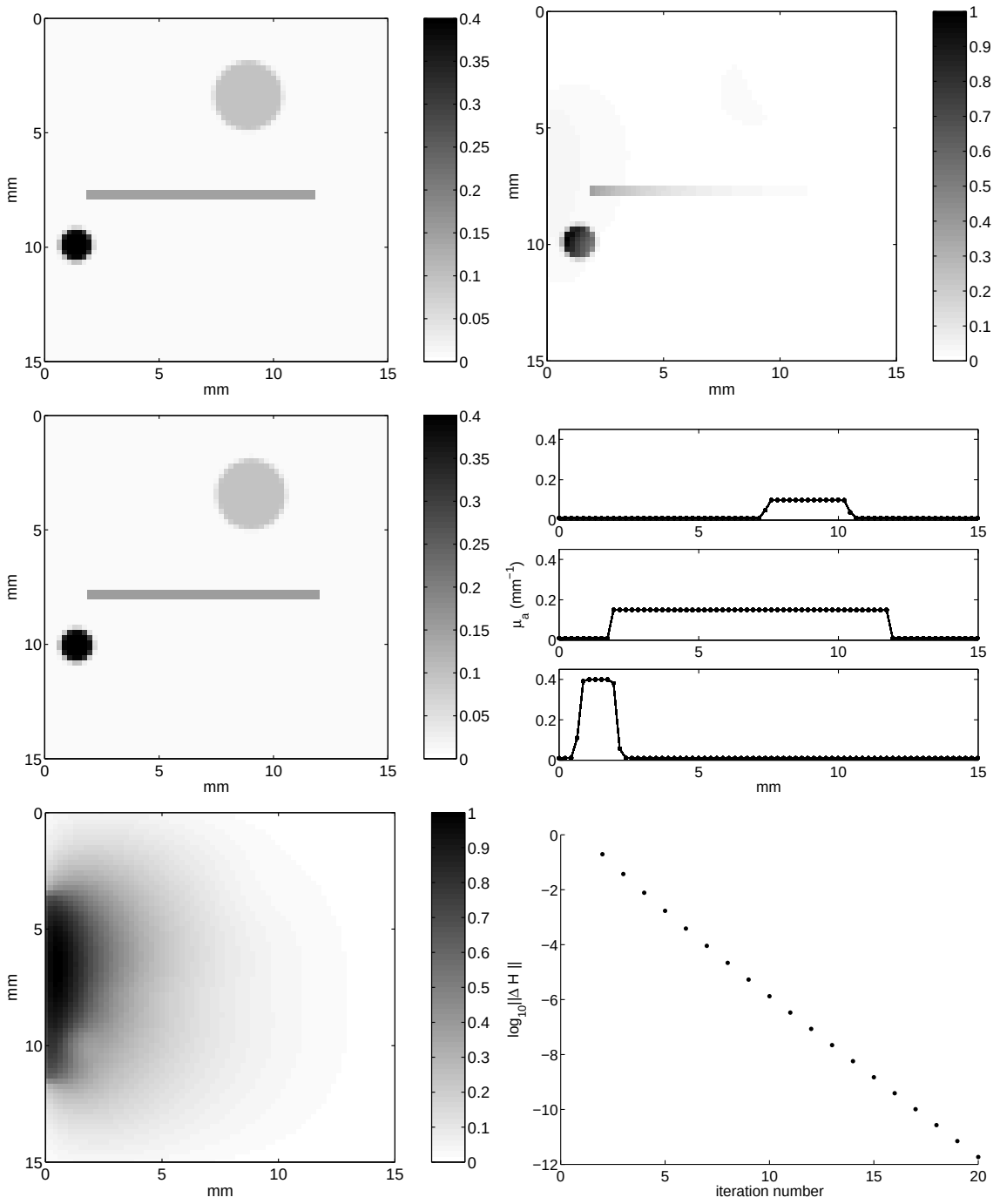

Figure 2. Noise-free example. An absorption coefficient distribution (top left) and the normalised absorbed energy map (top right) that would result from it. This is the image that would be obtained using conventional photoacoustic imaging. The recovered absorption map after 20 iterations (middle left). Horizontal slices through it at 3.5 mm, 7.8mm and 10.0 mm (middle right) give the true absorption (solid line) and the estimated absorption (dots). These show that the true absorption has been accurately recovered. The normalised fluence distribution is also shown (bottom left). A measure of the error in the estimates, $\log_{10} \|\Delta H\|$, decreases rapidly with increasing iteration number indicating convergence (bottom right).

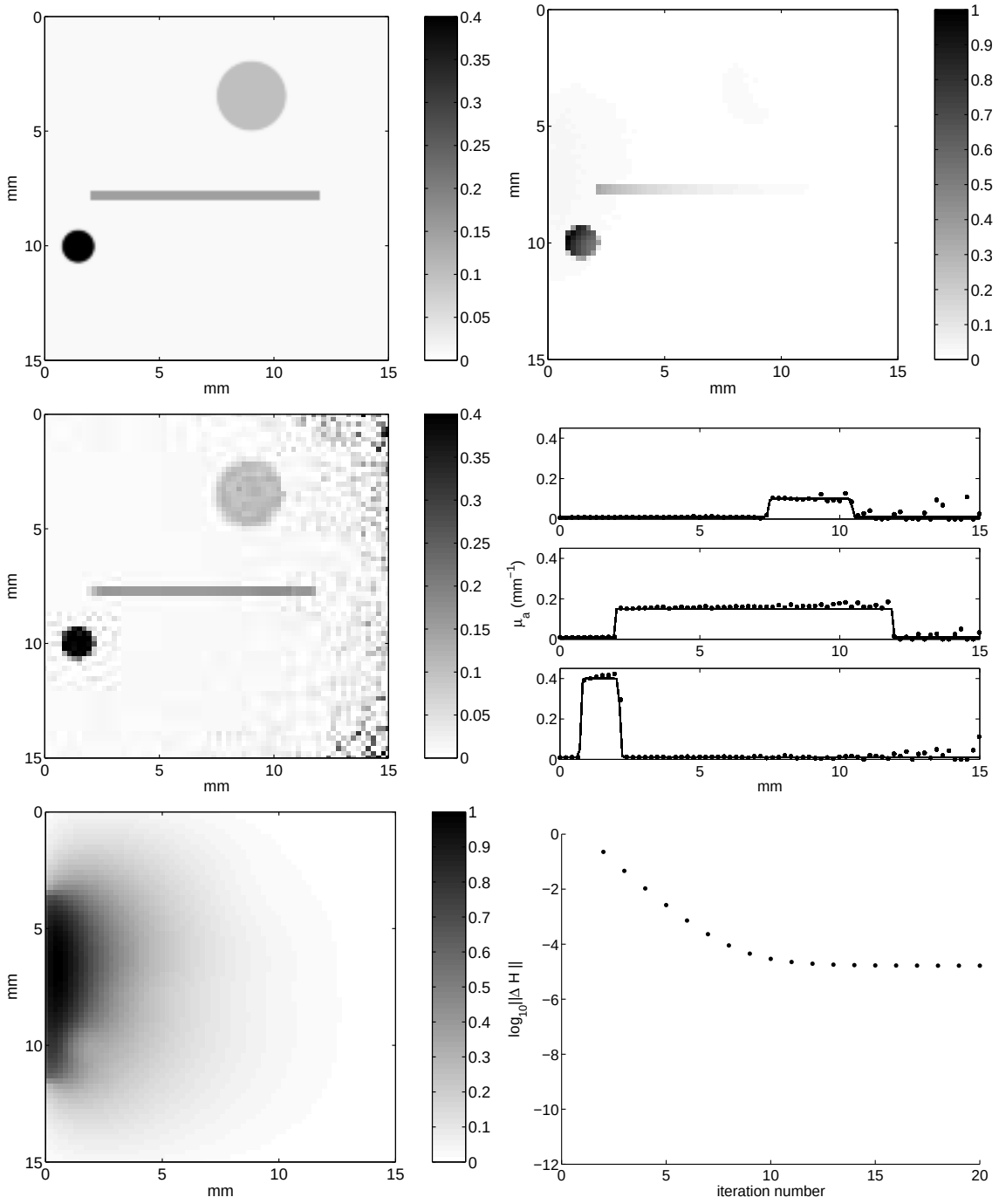

Figure 3. Noisy example. An absorption coefficient distribution on a 151 × 151 grid (top left). The 'measured' normalised absorbed energy map, including noise, on a 70 × 70 grid (top right). The recovered absorption coefficient distribution after 20 iterations (middle left) and horizontal slices through it at 3.5 mm, 7.8 mm and 10.0 mm (middle right). True absorption (solid line), estimated absorption (dots). The estimated fluence distribution (bottom left). The error measure $\log_{10} \|\Delta H\|$ against iteration number indicates convergence (bottom right).

4. CONCLUSION

An iterative algorithm that recovers the absorption coefficient distribution from the absorbed energy distribution - as provided by a conventional photoacoustic reconstruction algorithm - has been described. It has been shown to provide a good estimate of the absorption distribution using both noise-free and noisy simulated data. As the absorption coefficient distribution depends directly on tissue physiology, and not on the light fluence, this offers a means of producing an image contrast distribution that is more representative of the structure of the tissue. As the absorption coefficient distribution has been recovered, accurate spectroscopic imaging could be used to provide details of the distribution of specific chromophores.

The effect of uncertainty in the light source, measurement calibration and scattering distribution will be the subject of further work.

ACKNOWLEDGMENTS

This work was supported by the Engineering and Physical Sciences Research Council, UK and the Swiss National Science Foundation.

REFERENCES

1. J. Laufer, C. Elwell, D. Delpy, and P. Beard, "Pulsed near-infrared photoacoustic spectroscopy of blood," *Proceedings of SPIE* **5320**, pp. 57–68, San Jose, 2004.
2. J. Laufer, C. Elwell, D. Delpy, and P. Beard, "Spatially resolved blood oxygenation measurements using time-resolved photoacoustic spectroscopy," *Advances in Experimental Medicine and Biology* , 2005, in press.
3. R. Kruger, W. Kiser, D. Reinecke, G. Kruger, and K. Miller, "Thermoacoustic optical molecular imaging of small animals," *Molecular Imaging* **2**, pp. 113–123, 2003.
4. G. Paltauf and H. Schmidt-Kloiber, "Pulsed optoacoustic characterization of layered media," *Journal of Applied Physics* **88**(3), pp. 1624–1631, 2000.
5. K. P. Köstli, M. Frenz, H. Bebie, and H. P. Weber, "Temporal backward projection of optoacoustic pressure transients using Fourier transform methods," *Physics in Medicine and Biology* **46**(7), pp. 1863–1872, 2001.
6. K. Köstli and P. Beard, "Two-dimensional photoacoustic imaging by use of Fourier-transform image reconstruction and a detector with an anisotropic response," *Applied Optics* **42**(10), pp. 1899–1908, 2003.
7. M. H. Xu, Y. Xu, and L. H. V. Wang, "Time-domain reconstruction-algorithms and numerical simulations for thermoacoustic tomography in various geometries," *IEEE Transactions on Biomedical Engineering* **50**(9), pp. 1086–1099, 2003.
8. X. Wang, Y. Pang, G. Ku, X. Xie, G. Stoica, and L. V. Wang, "Noninvasive laser-induced photoacoustic tomography for structural and functional in vivo imaging of the brain," *Nature Biotechnology* **21**(7), pp. 803–806, 2003.
9. A. J. Welch and M. van Gemert, *Optical-Thermal Response of Laser-Irradiated Tissue*, Plenum Press, New York, 1995.
10. S. Arridge, M. Schweiger, M. Hiraoka, and D. Delpy, "A finite element approach for modelling photon transport in tissue," *Medical Physics* **20**, pp. 299–309, 1993.